Snowfall Associated with a Terrain-Generated Convergence Zone during the Winter Icing and Storms Project

DOUGLAS A. WESLEY,* ROY M. RASMUSSEN, AND BEN C. BERNSTEIN

Research Applications Program, National Center for Atmospheric Research,† Boulder, Colorado

(Manuscript received 9 May 1994, in final form 27 March 1995)

ABSTRACT

The Longmont anticyclone, a region of low-level anticyclonic turning and convergence during episodes of northerly winds along the Front Range of the Rocky Mountains, is documented for a snow event that occurred during the Winter Icing and Storms Project. The complex terrain in this region, especially the barrier to the west and the sloping Cheyenne Ridge to the north, is critical for the formation of this mesoscale feature. Upward motions related to this persistent convergent region downstream of the Cheyenne Ridge can strongly influence local snowfall distributions. The particular event studied in this manuscript was weakly forced on the synoptic scale. Through close examination of Doppler radar, special sounding and surface mesonetwork data, the effects of the Longmont anticyclone on snowfall were determined. The results of the analyses suggest that the convergence triggered convective snowbands in a region of delayed postfrontal cold advection at low levels. A series of mesoscale model simulations predicted the behavior of low-level northerly flow along the Front Range and demonstrated the role of the terrain during the development of the Longmont anticyclone. The results of these simulations were compared to the case study results.

1. Introduction

Closely spaced surface, sounding and radar measurements in northeastern Colorado have made possible the detection and analysis of terrain-generated circulations and low-level convergence zones. An excellent example is the so-called Denver cyclone or convergence–vorticity zone, a common feature over the eastern plains of Colorado associated with the development of severe thunderstorms and snowbands (Szoke 1991; Rasmussen et al. 1992; Wilczak and Christian 1990). It can occur when the low-level flow over the plains is southerly or southeasterly, and it affects storm initiation and evolution in the Denver area.

The existence of cyclonic mesoscale vortices in mountainous terrain that strongly influence local weather and pollutant transport has been well documented in many locations, as summarized by Wilczak and Christian (1990). However, their counterpart, anticyclonic terrain-induced features, have not received as much attention. Model simulations of airflow past the island of Hawaii by Smolarkiewicz et al. (1988) and Reisner and Smolarkiewicz (1994) produced cyclonic and anticyclonic eddies to the lee of the island. Associated with both eddies were significant pockets of upward motion and condensation. Though cloud features associated with the anticyclonic eddy had not been emphasized in previous field studies, Fig. 2 in Smolarkiewicz et al. (1988) showed a cluster of cloudiness located downstream of the south side of the island in close proximity to the updrafts and anticyclonic eddy predicted in the simulations. The tendency for low-level anticyclonic flow to occur to the lee of the left side (facing downstream) of a three-dimensional obstacle was in agreement with predictions of several theoretical studies of low–Froude number flow. These studies of stratified flow explain anticyclonic turning to the lee of the obstacle as being produced by the tilting of horizontal vorticity into the vertical by the horizontal shear in the wind (Reisner and Smolarkiewicz 1994; Snook 1993; Crook et al. 1990; Smolarkiewicz and Rotunno 1989). Nickerson and Dias (1981) also reported that both anticyclonic and cyclonic vortices occurred on the downwind south and north sides of Hawaii, respectively. The low-level flow accelerated around each side of the island and converged on the lee side with essentially stagnant conditions. The vortices generated stratiform cloudiness below the trade-wind inversion. Akaeda et al. (1993) studied precipitation patterns to the lee of Taiwan, and found that terrain-induced convergence on the lee side often enhanced precipitation. A significant mesoscale feature in western Washington

* Current affiliation: National Weather Service, Cheyenne, Wyoming.

† NCAR is sponsored by the National Science Foundation.

Corresponding author address: Dr. Douglas A. Wesley, National Weather Service, 1301 Airport Parkway, Cheyenne, WY 82001-1549.
E-mail: Douglas_Wesley_at_W-CR-CYS@smtpgate.ssmc.noaa.gov

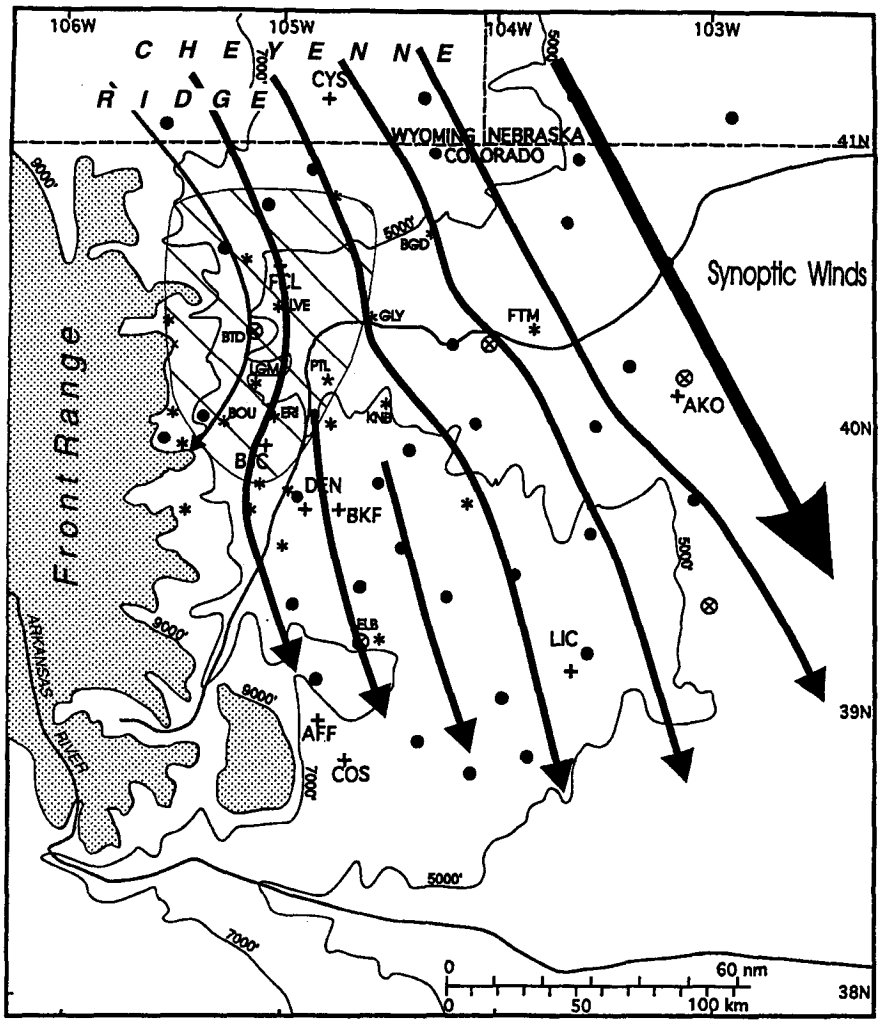

FIG. 1. Schematic of the general low-level wind flow present during the Longmont anticyclone event of 16 January 1991. Solid contours indicate elevation, and areas above 2.75 km are shaded. The hatched area indicates the region of anticyclonic turning and convergence (see text). A portion of mesonetwork and SAO locations are included: CYS: Cheyenne; FCL: Fort Collins; DEN: Denver; BKF: Buckley Field; BJC: Jeffco Airport; AFF: Air Force Academy; COS: Colorado Springs; AKO: Akron; LIC: Limon; FTM: Fort Morgan; ELB: Elbert; KNB: Keenesburg; GLY: Greeley; ERI: Erie; BOU: Boulder; LGM: Longmont; PTL: Platteville; BTD: Berthoud; LVE: Loveland; BGD: Briggsdale.

is the Puget Sound convergence zone (Ferber and Mass 1990), part of which is a region of anticyclonic turning and deceleration downstream of an isolated mountain. This turning leads to north winds, and convergence of this northerly flow with leeside southwesterlies often produces clouds and precipitation in this region. Marwitz and Dawson (1984) documented anticyclonic turning in westerly boundary layer winds downwind of the Medicine Bow Mountains in southeastern Wyoming. The resulting northwesterly flow frequently converged with low-level southwesterly winds originating in north-central Colorado along a northwest to southeast line extending about 100 km downwind of the eastern edge of the barrier. Stably stratified conditions existed upstream of the barrier. In addition, an anticyclonic eddy downwind of a smaller mountain northwest of the Medicine Bow range was described in that study.

An anticyclonic eddy forms to the lee of the Cheyenne Ridge (a ridge extending eastward from the Rocky Mountains along the Wyoming–Colorado border) when the flow upstream of the ridge is northerly or northwesterly. Figure 1 presents a schematic of the low-level flow. The feature was first documented by Johnson et al. (1984) as a "surface anticyclonic circulation. . . downstream of the Cheyenne Ridge when a northwesterly gradient wind in the lower troposphere

exists over the area." Their Fig. 8c demonstrates anticyclonic turning to the lee of the Cheyenne Ridge and the colder temperatures characterizing the region of northwesterly winds. Denver soundings in that study showed highly ageostrophic upslope winds from the surface up to nearly 600 mb. This flow was speculated to be related to mesoscale circulations produced by both the leeside anticyclonic turning and differential surface heating between snow-covered and snow-free areas. Although no term has been officially coined for this phenomenon, forecasters in this region refer to it as the Longmont anticyclone, with the geographical reference specifying the preferred approximate location of the center of the region of strongest anticyclonic turning [see the location of Longmont (LGM) in Fig. 1].

During the winters of 1990 and 1991 the Winter Icing and Storms Project (WISP) was conducted in northeastern Colorado (see Fig. 1 and Rasmussen et al. 1992). Investigators from a number of universities, as well as from NCAR and NOAA, documented the evolution of supercooled liquid water during winter storms in this region of complex terrain using data collected at the surface and aloft. One major objective of this project was to evaluate the effects of topography on snowfall distributions. Preliminary analyses of all WISP intensive observing periods (IOPs) in 1990 and 1991 have brought to light a noteworthy result. Out of 25 total IOPs during the 2-yr period, the Longmont anticyclone (LA) appeared to be present during the evolution of snowbands or convective snow-producing regions for 16 events. Of these events, the LA appeared to be especially important in several light snowfall IOPs.

The generalized schematic shown in Fig. 1 presents one example of the low-level wind pattern associated with the LA, based primarily on the case study discussed in this manuscript. Following the passage of a cold front of either Canadian or Pacific origin, a period of gusty northerly surface winds typically occurs over the eastern plains of northern Colorado and southeastern Wyoming, accompanied by northwesterly midlevel flow. The observed northerly surface winds are partially isallobaric in nature, with surface pressures rising rapidly over eastern Wyoming. For time periods of a few or more hours, the northerly or northwesterly low-level flow in the lee of the Cheyenne Ridge (the central axis of which is located just north of the Colorado–Wyoming border) turns anticyclonically and decelerates. The hatched region of Fig. 1 specifies a region of convergent northerly flow. The convergence in the low-level flow in this region may generate convection and showery precipitation, depending on the atmospheric stability and moisture profiles, while partly cloudy, nonprecipitating conditions are observed elsewhere over the plains. In some situations, preexisting precipitation bands advecting into this region may intensify as they move across the region of low-level convergence. Significant precipitation can occur over the Boulder–Longmont–Platteville–Denver (BOU–LGM–PTL–DEN in Fig. 1) areas during LA situations, despite the shallow, anticyclonic nature of the postfrontal air mass and the lack of significant upslope during north to northwesterly winds at the surface. This scenario can occur during any season. In some cases, the anticyclonic turning shown in Fig. 1 may be more pronounced, with persistent *southerly* breezes observed in the Fort Collins–Loveland vicinity (Johnson et al. 1984) resembling return flow.

The 16 January 1991 episode was chosen in this study for detailed analysis due to the persistent intensification of snowbands via low-level convergence associated with the LA and due to the lack of significant large-scale dynamical forcing. The total snowfall was light in this case but it presented an excellent opportunity to study the effects of terrain without the complications of ascent produced at larger scales. The purpose of this paper is to document the LA for this case, and especially to demonstrate its effect on the snowfall distribution. WISP instruments and locations are described briefly in section 2. Detailed analyses of the structure of the LA using surface and sounding data for the case study are presented in section 3. The effects of the LA on the precipitation are described in section 4. Section 5 presents results of mesoscale model simulations of the LA. In section 6, we discuss possible mechanisms leading to precipitation enhancement associated with the LA. Section 7 presents the conclusions.

2. Data sources

The 1991 Winter Icing and Storms Project took place in northeastern Colorado from 15 January through 1 April (see Rasmussen et al. 1992). Figure 1 presents the locations of major geographical features. Primary data sources for this study included a network of 39 NCAR Portable Automated Mesonet (PAM) and 22 NOAA/PROFS mesonet instruments, which continuously measured surface pressure, temperature, dewpoint, and winds. Six Cross-chain Loran Atmospheric Sounding Systems (CLASS) were strategically placed within the PAM network; balloons were released at 3-h intervals during IOPs. In addition, soundings were taken by a mobile CLASS van, in this case located 30 km south-southeast of Greeley (GLY). The Colorado State University CHILL, University of North Dakota (UND), and Mile High (MHR) Doppler radars provided coordinated conical volumes of reflectivity and radial velocity fields. Further details on WISP observing systems are discussed in Rasmussen et al. 1992.

3. The 16 January 1991 event: A case study of the structure of the Longmont anticyclone

This section first describes the large-scale conditions associated with the development of the LA in this case

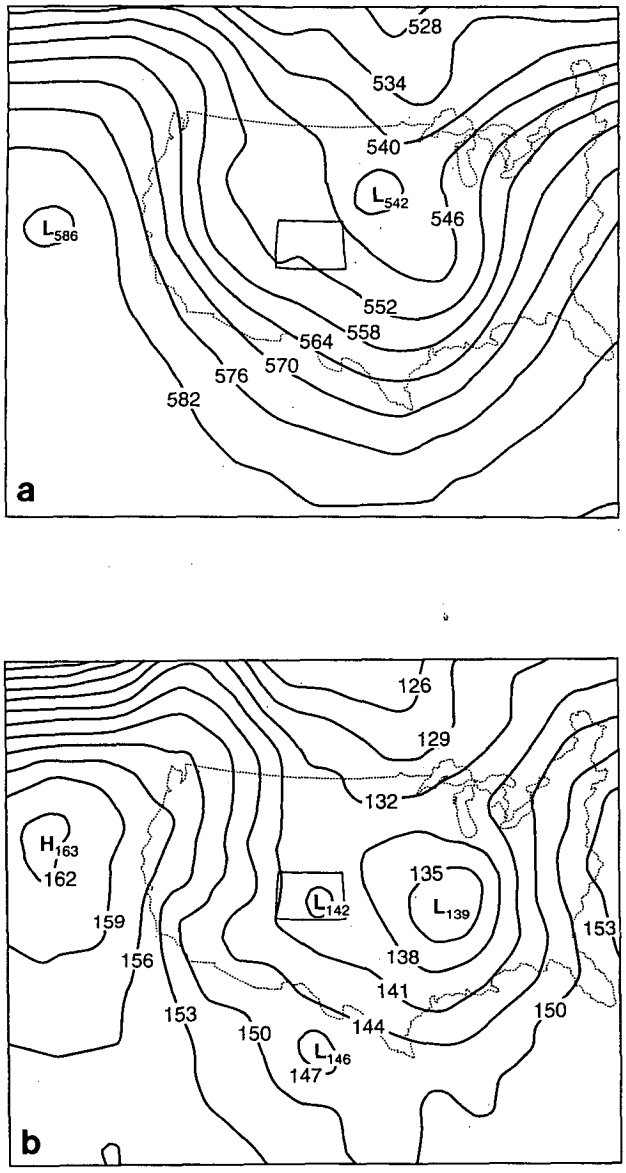

FIG. 2. NMC (a) 500-mb analysis and (b) 850-mb analysis at 0000 UTC 16 January 1991. Solid contours are heights (dam). The state border of Colorado is outlined.

and then examines the small-scale flow and stability structure.

a. Synoptic situation

At 1200 (all times UTC) 15 January 1991 Colorado was experiencing northwesterly flow at 500 mb on the back side of a large-amplitude trough over the central High Plains of the United States. By 0000 UTC 16 January northwest winds at 500 mb over Colorado weakened significantly and heights fell slowly as a weak trough axis moved southward west of Colorado (Fig. 2a). Flow at 700 mb over Colorado was also relatively weak and northwesterly. The 850-mb analysis at this time (Fig. 2b) indicated that a low pressure trough was forming in central Arizona at this time in response to the approach of the intensifying wave. A weak cold front associated with the approach of the trough axis passed southward through the WISP domain by 0200. At 0400, low cloud covered most of eastern Colorado and eastern Wyoming. Over the next 8 h, both regions were characterized generally by scattered light snow showers and varying degrees of low cloud coverage, ranging from obscured conditions to partly cloudy skies. Surface pressures rose significantly during this time (up to 15 mb in 12 h) over Wyoming. As seen in the enhanced infrared satellite image at 0600 (Fig. 3a), colder cloud-top temperatures (CTTs),

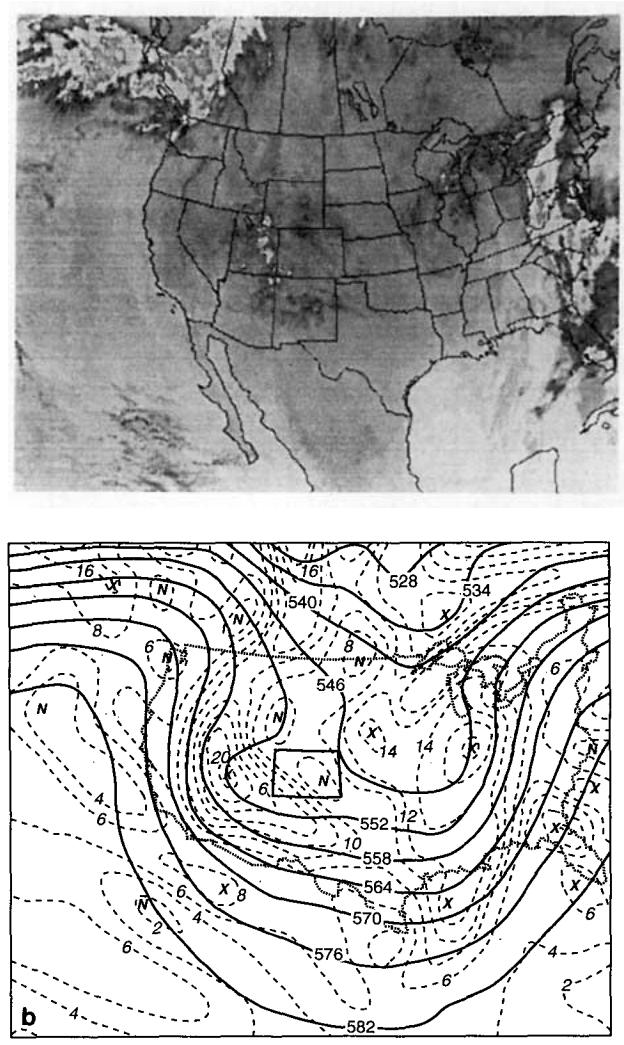

FIG. 3. (a) Enhanced infrared satellite image at 0600 UTC 16 January. Lightest gray shading corresponds to cloud-top temperatures less than −60°C. Cloud-top temperature over northeastern Colorado is approximately −20° to −35°C. (b) Six-hour NGM forecasts of 500-mb vorticity ($\times 10^{-4}$ s^{-1}) (dotted lines) and heights (dam) for 0600 UTC 16 January.

which correspond to the lighter gray shading in the figure for values less than −45°C, were confined to extreme southwestern Wyoming, eastern Utah, and the Four Corners region. These CTTs represented deep cloudiness associated with the active portion of the upper-level trough. A 6-h forecast of 500-mb vorticity and heights for the Nested Grid Model (NGM) valid at 0600 is shown in Fig. 3b. The center of the deepening trough was located over southern NV at this time, or just west of the colder CTTs. Strong high-level winds were far removed from the area of interest (northeastern Colorado) throughout this period, so that jet streak dynamics were not a factor. Further examination of thickness (not shown) and vorticity analyses did not reveal significant advection of vorticity by the thermal wind over eastern Colorado nor appreciable values of differential vorticity advection. Also thermal advection fields aloft were relatively weak. Six-hour vertical velocity predictions by the NGM over the region for 0600 (not shown) indicated no significant ascent predicted for the midlevels over the region. All of these data indicate that significant large-scale forcing was apparently confined to regions well west and south of the WISP project area. Weak large-scale forcing simply set up ageostrophic northerly low-level winds over northeastern Colorado, along with high relative humidity and cold advection in the lower troposphere.

b. The mesoscale: An overview of PAM and CLASS data

This subsection summarizes analyses of WISP measurements during the period of interest, 0300–1200 UTC 16 January, with an emphasis on the structure and evolution of the LA. The surface cold front progressed through the surface mesonetwork between 2100 UTC 15 January and 0200 UTC 16 January and signaled the onset of weak low-level cold advection. Upon frontal passage, low-level northwesterly winds switched to northerly but did not strengthen appreciably.

1) SURFACE MESONETWORK ANALYSES

An objective analysis of the surface mesonet winds and convergence at 0400 showed that northerly winds dominated the northern half of the WISP domain (Fig. 4). During the 2-h period between 0300 and 0500, winds at BOU, LGM, and BTD became nearly calm as convergence associated with the LA developed. An area of significant convergence, with magnitudes up to 1.5×10^{-4} s^{-1}, had developed from just north of FCL south-southeastward to east of DEN. The divergence field 1 h earlier (not shown) was very similar. The surface pressure analysis using the high-resolution observations (Fig. 5b) showed that generally a northwest–southeast gradient was present, in agreement with the large-scale analysis (Fig. 5a). However, in the northwest portion of the WISP domain the pressure gradient was nearly nonexistent. This reduced pressure gradient will be discussed later in this manuscript. At 0700 (Fig. 6), winds south of the western South

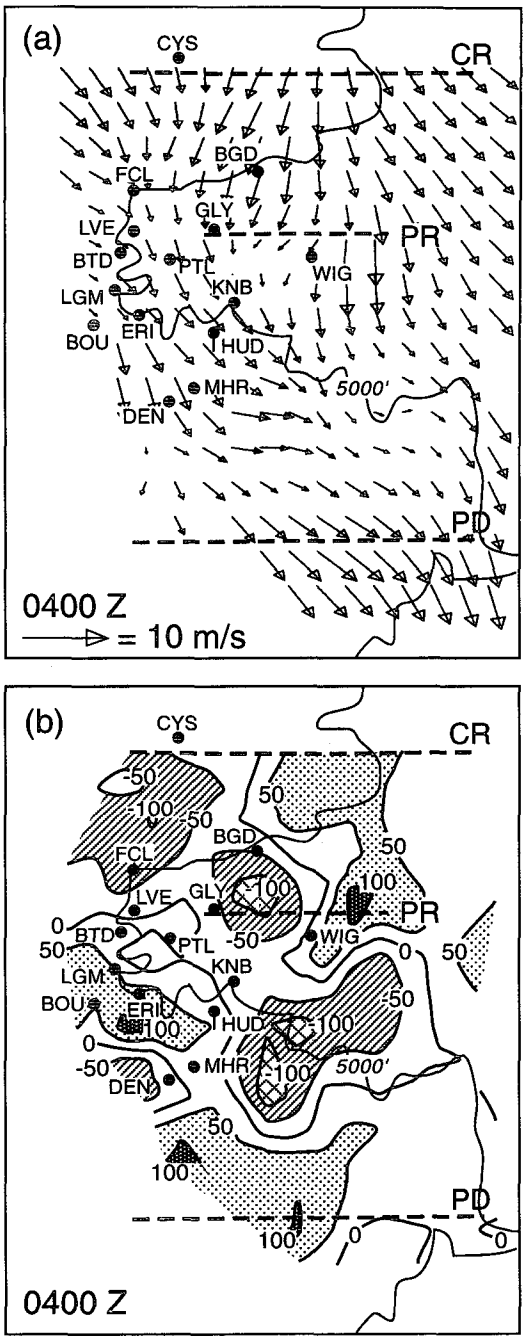

FIG. 4. (a) Objective analysis of PAM and PROFS wind observations at 0400 UTC 16 January. Vectors indicate wind speed and direction. Dotted lines indicate approximate locations of the Cheyenne Ridge (CR), the South Platte River valley (PR), and Palmer Divide (PD). Solid line denotes the approximate location of the 1.52-km (5000 ft) elevation contour. (b) Divergence calculated from surface observations in (a). Contour interval is 5×10^{-5} s^{-1}.

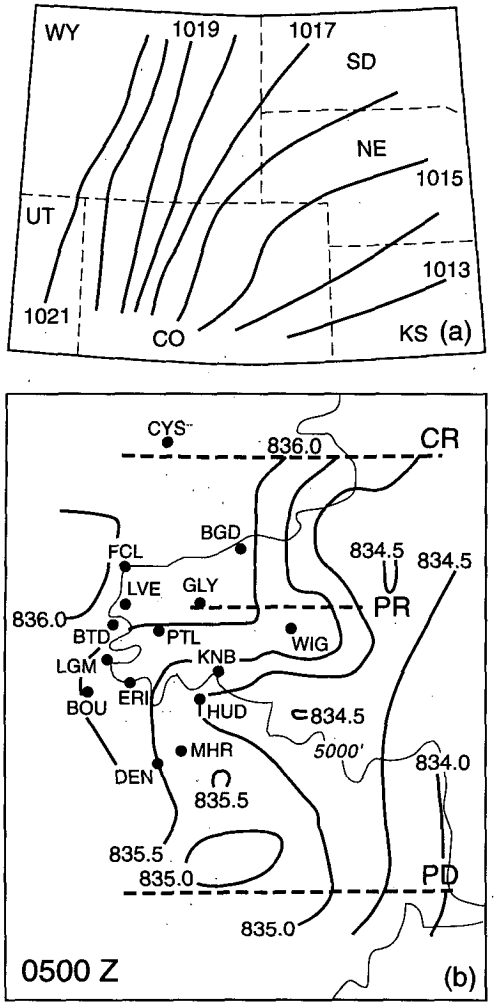

FIG. 5. (a) MSL pressure (mb) analysis at 0700 UTC 16 January. (b) Mesonetwork pressure (mb) analysis at 0500 UTC 16 January. Values are reduced to an intermediate elevation, 1600 m, using a temperature lapse rate determined by the PAM measurements.

Platte River valley (note: this geographical reference throughout this manuscript applies to the approximate area inside a polygon defined by the FCL, ERI, KNB, and GLY locations in Fig. 1) increased and steadily turned cyclonically back to north-northwesterlies as they ascended the Palmer Divide. Note that at this time the winds over the eastern plains (east of approximately WIG and BGD) were primarily from the northwest. Though anticyclonic turning and deceleration were both significant at this time, there was little evidence of fully developed return flow—that is, southerlies—along the foothills, in contrast to the study of Johnson et al. (1984). Major convergent regions at 0600 and 0700 were located mainly over the foothills and immediate adjacent plains from FCL to BTD (see Fig. 6c). An analysis of the surface potential temperature at 0700 (Fig. 6b) revealed the presence of potentially warmer air near the foothills west of FCL and LVE where the flow was decelerated.

Calm conditions still dominated the BOU–LGM–DEN region at 1200; in fact the BOU and LGM sites remained calm until after 1600, when winds finally became north-northwesterly there. Surface dewpoint observations at Cheyenne (CYS) were persistently around −4°C (with temperatures only slightly higher) between 2300 UTC 15 January and 1400 UTC 16 January, after which the dewpoint fell significantly. Subsequent mesonetwork data indicated a reappearance of a marked LA around 1900 to 2000, although the lack of sufficient low-level moisture prevented significant cloud development during this time.

2) AVERAGED WINDS

Temporal averaging of the mesonet winds in this case proved to be an effective tool in generalizing the LA wind pattern. Figure 7a shows the vector average of the mesonetwork surface winds over the 4.5-h time period between 0430 and 0900, the most active period of precipitation. This plot indicated that north-northwesterly winds over the Cheyenne Ridge, averaging about 5 m s^{-1}, persistently decelerated and turned anticyclonically by about 40° to the lee of this feature in the FCL–BOU–GLY region. The average reduction in wind speed over the western South Platte Valley was about 3 m s^{-1}, whereas winds elsewhere in the mesonet were relatively unaffected. There is also evidence in Fig. 12a of some convergence between westerly flow in the foothills northwest of DEN and northerly flow on the plains east of BOU and LGM. Areas of significant convergence during this period (Fig. 7b) were located from the foothills west of FCL northeastward to NUN.

3) SOUNDINGS

Vertical thermodynamic and wind profiles were measured at six locations during the 16 January 1991 event (see Fig. 1), enabling further assessment of wind characteristics and lapse rates associated with the LA. These observations were critical for understanding the role of low-level instability in the development of snowfall, which will be discussed further in section 4.

The Berthoud (BTD) site was located within the convergence zone, a short distance to the lee of the Cheyenne Ridge and near the foothills. The first BTD profile, shown in Fig. 8a, was launched at 0414 as the LA was developing. Due to mechanical problems with this sounding, winds were only recorded in the lowest 250 mb, but thermodynamic data were measured through the troposphere. Aside from a shallow ground-based stable layer, the lapse rate was approximately dry adiabatic up to about 690 mb. Dewpoint depressions were 3°C or less from the surface to about 500 mb, and nearly zero in a cloudy layer from about 730 to 690

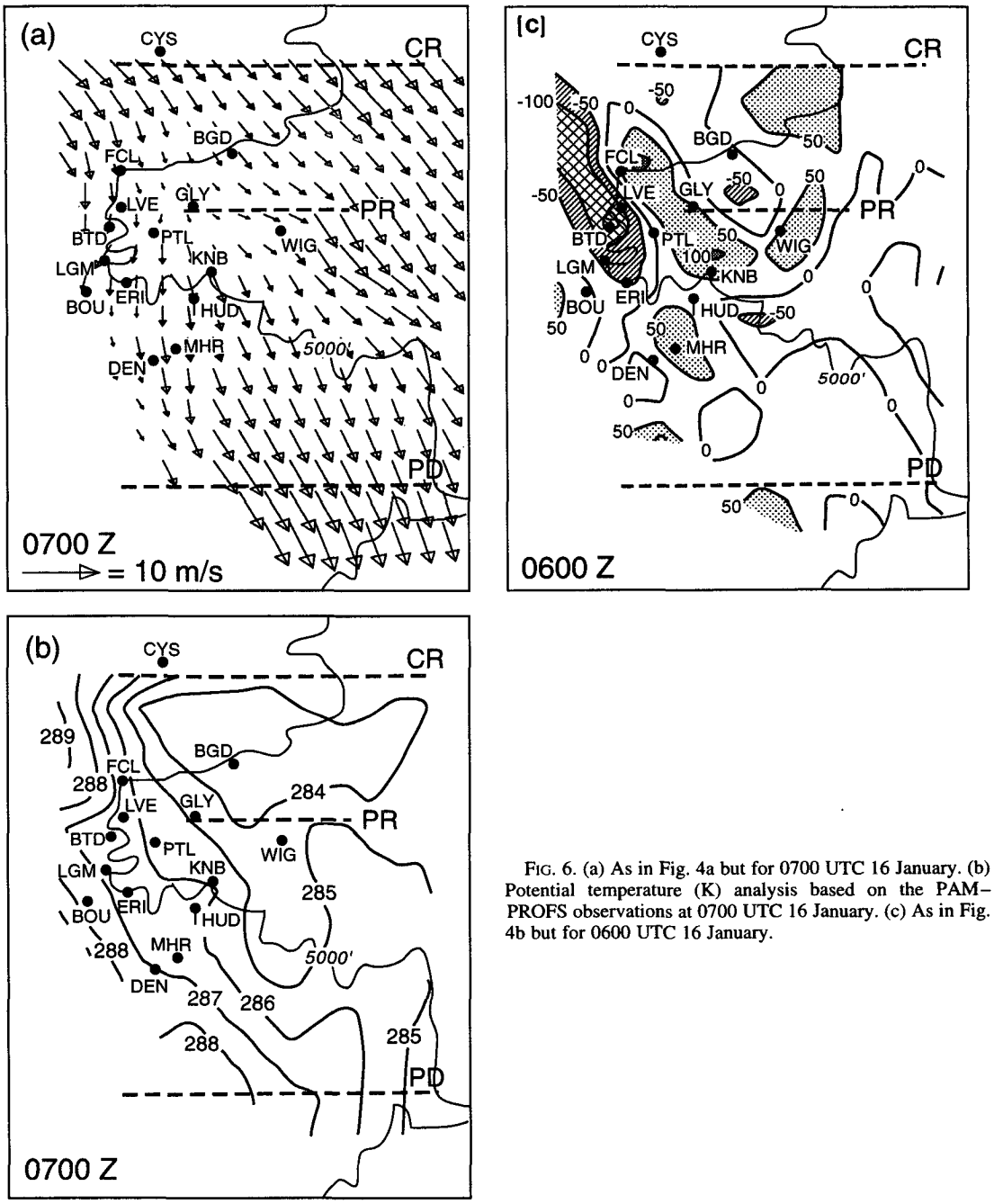

FIG. 6. (a) As in Fig. 4a but for 0700 UTC 16 January. (b) Potential temperature (K) analysis based on the PAM–PROFS observations at 0700 UTC 16 January. (c) As in Fig. 4b but for 0600 UTC 16 January.

mb. The shallow stable layer near the surface was verified by mesonetwork temperature measurements and close examination of the CLASS data points within it. The layer may have been caused by radiational cooling during the previous several hours, which were characterized by light winds; also some residual snow cover was in the vicinity, which could have accentuated the shallow nocturnal inversion. Detailed discussion of the BTD thermodynamic profiles is presented in the appendix.

Lapse rates and relative humidity measurements above the low-level inversion indicated that the potential for convection existed at 0414. The available wind data shows predominantly northerly flow, steadily increasing from nearly calm at the surface to about 10 m s^{-1} between 775 and 630 mb. At Hudson (HUD) (about 30 km to the southeast of BTD) the low-level lapse rate at 0314 (not shown) was much more stable than that at BTD (0414). A shallow layer of northeasterly flow was present, consistent with the early

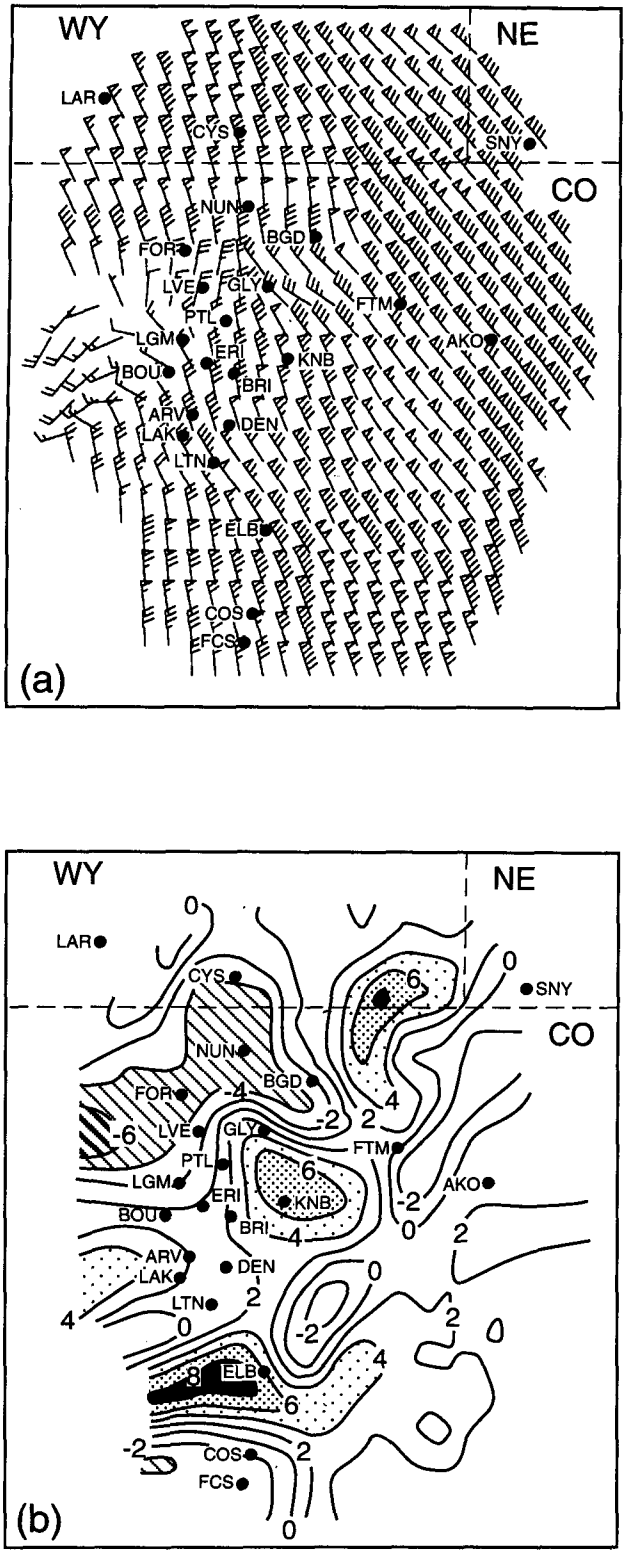

FIG. 7. (a) Time average of PAM–PROFS wind observations between 0430 and 0900 UTC 16 January. One wind barb equals 1 kt; one flag equals 5 kt. Locations are as in Fig. 1. Thin black lines are state boundaries. (b) Surface divergence for observations in (a). Contour interval is 2×10^{-4} s^{-1}.

stages of the LA as discussed previously. Winds backed about 60° and strengthened slightly between the surface and 600 mb.

The BTD 0610 sounding (see Fig. 8b) was taken during the most significant LA convergence period and likely represents a typical sounding during the LA at that location. Moderate snowfall was occurring at BTD. A moist and unstable layer existed from above the ground-based shallow inversion to about 720 mb. From the 720-mb level upward, more stable conditions were measured as the lapse rate became nearly moist adiabatic. Conditions were nearly saturated up to about 600 mb. A shallow (about 500 m deep) layer of northeasterly flow of 4–6 m s^{-1} was present just above the surface, and coincided with the *warmest* layer in the sounding. The wind direction subsequently backed to primarily northerly flow by 780 mb, and strengthened to 10–15 m s^{-1}.

The lower layer of northeasterlies in the BTD profile at 0610 appeared to be the signature of the LA. Regions north of BTD, over and on the immediate south side of the Cheyenne Ridge, did not experience northeasterly winds at the surface as noted previously. Convective instability was readily evident in the lapse rate and moisture content in the lower troposphere at BTD. With a small amount of lifting, convection could easily occur. Radar echoes (to be discussed later) persistently contained relatively small cellular features of significant depth, and WISP aircraft measured convectively unstable profiles in this region.

The MHR 1.2° velocity scan at 0700 (not shown) measured a radial wind component toward the radar of 15–20 m s^{-1} in the vicinity of BGD (at a height of approximately 3.2 km MSL) decreasing to 5–10 m s^{-1} over and near the foothills just west of LVE. Soundings just prior to this time at BTD and WIG measured wind directions of approximately 340° at this height. The actual wind encountered by MHR over BTD was thus nearly aligned along a radial, while 50 km to the east (near BGD) the wind was angled sharply away from the radial direction. Thus it is likely that winds at a height of approximately 3.2 km MSL were much weaker along the foothills north of BOU than out on the plains. This implied that the decelerated flow associated with the LA extended well above the surface.

The final BTD release at 0900 (not shown) revealed that the lower layers of the troposphere had stabilized significantly since 0610. CTTs were increasing during this period. The lowest 20–30 mb of the atmosphere still experienced weak easterly winds (within a much shallower layer than at 0610), but low- and midlevel drying had occurred and dewpoint depressions had increased by 3°–6°C from the surface to 550 mb. Precipitation activity (inferred from MHR and discussed later) had diminished significantly in this region during the 0800–0900 time period. No soundings were launched from this site after 0900.

Wiggins (WIG) was east of the LA convergence zone during the period of interest. The CLASS release at that location at 0615 (see Fig. 8c) measured about 30° of backing of winds with height between 700 and 500 mb and no easterly component below 400 mb. Surface winds were northerly, and the lowest 100 mb was much drier than that of the 0610 BTD profile. At 0900 (not shown), more drying was evident throughout the 850–500-mb layer at WIG, and low-level northerlies had strengthened. At AKO, which is located far enough to the east to be relatively unaffected by the LA, CLASS profiles also lacked any easterly component in the lower layers.

The 915-MHz profiler at DEN measured wind profiles continuously in the southern portion of the LA during this event. Hourly data (not shown) indicated a persistent layer of north-northeasterly winds, of speeds 7.5–15 m s^{-1}, between 810 and 720 mb. The period of strongest easterly component (wind direction approximately 020°) occurred at DEN during the 0400–0800 time period, which corresponded with the strongest period of the LA.

4. Snowbands and the 16 January 1991 Longmont anticyclone

Three snowbands developed during the period 0300–1300 UTC 16 January 1991. In this section the behavior of the snow-producing features in relation to the location and structure of the LA are described in detail. Generally, snowbands developed to the lee of the western portion of the Cheyenne Ridge and propagated southward through the WISP domain.

a. Initial snowband (B1)

During the early stages of the LA (0300–0600) a snowband developed and intensified within the WISP domain. The 2.0 km (all heights MSL) CAPPI (constant-altitude plan position indicator) of Mile High Radar (MHR) reflectivity at 0330 (Fig. 9a) indicated the initiation of an active precipitation pattern, with a newly developed snowband (denoted hereafter as B1) with reflectivity values of 15–25 dBZ extending from east of FCL southeastward toward PTL. Here B1 was moving southward. Other significant features were pockets of reflectivity up to 30 dBZ, to the west and south of Denver. Low-level reflectivity features at 0600 (not shown) included areas of 30 dBZ associated with B1 located just east, north, and northeast of DEN. As discussed previously, by 0600 a pronounced LA was present with significant convergence over the foothills and immediately adjacent plains northwest of Denver. At 0700, DEN reported light snow, which continued over the next 2 h. Only light snow showers were reported before this time.

b. Snowband B2

A new band (hereafter called B2) began to develop rapidly near LVE between 0600 and 0700 in the convergent region discussed previously. A CAPPI at 0701 (Fig. 9b), when the strongest signature of the LA was present, showed an organized band (B2) of enhanced reflectivity oriented east-southeast to west-northwest extending from just south of LVE to northeast of DEN. The band exhibited several cellular features with reflectivity values up to 30 dBZ. The eastern edge of B2 was clearly defined about 30 km east-northeast of MHR. The western end of this band contained an extension of reflectivity toward the north, with 25-dBZ echoes extending northward along the foothills well beyond BTD. This band was propagating southward at 11 m s^{-1}. UND radar data showed that 20-dBZ echoes within B2 reached heights of about 5.5 km, or near 500 mb, at this time.

A dual-Doppler analysis of reflectivity and band-relative wind fields from CHILL and MHR at 0705 provided more detailed information on the three-dimensional structure of B2. A north–south cross section through B2 at a distance of 28 km west of MHR (Fig. 10; see Fig. 9b for the geographical location of the cross section) showed that B2 was composed of several strong vertical extensions of reflectivity, with a maximum height of about 7 km. These appeared to be convective cells. The derived velocities showed that these extensions were associated with updrafts, the strongest of which was located about 10 km north of the latitude of MHR and exhibited updraft velocities in excess of about 0.5 m s^{-1}. The cross section contained a low-level region of reflectivity greater than 25 dBZ, and low-level band-relative inflow of about 5–6 m s^{-1}. The leading edge of B2 exhibited a layer of convergence about 2 km deep.

The Wyoming King Air instrumented aircraft conducted a flight through B2 between 0620 and 0707 within the dotted triangle shown in Fig. 9b (note that the radar scan shown in Fig. 9b occurred 40 min after the start of the flight through B2; thus B2 was about 25 km north of its position shown in Fig. 9b at the beginning of the flight), well after the period of rapid intensification of B2. Figure 11 shows the vertical cross sections for five different meteorological fields along the flight path. The data are distance adjusted for southward advection of the band. The measurements indicated that B2 resembled a long-lived southward-propagating convective line. The north–south wind component, shown in Fig. 11a, demonstrated that the low-level band-relative inflow was 5–6 m s^{-1}, in good agreement with the dual-Doppler analysis in Fig. 10. Convective instability (i.e., θ_e decreasing with height, Fig. 11b) was present between 3.0 and 5.0 km in height and between 10 and 40 km north of MHR, ahead of and within the leading portion of the band. High condensate supply rates associated with the updraft led to the production of small amounts of liquid water below 3.5 km (Fig. 11c) and large numbers of ice crystals higher up in the cloud (Fig. 11d). Maximum crystal concentrations were above 14 L^{-1} in a narrow zone

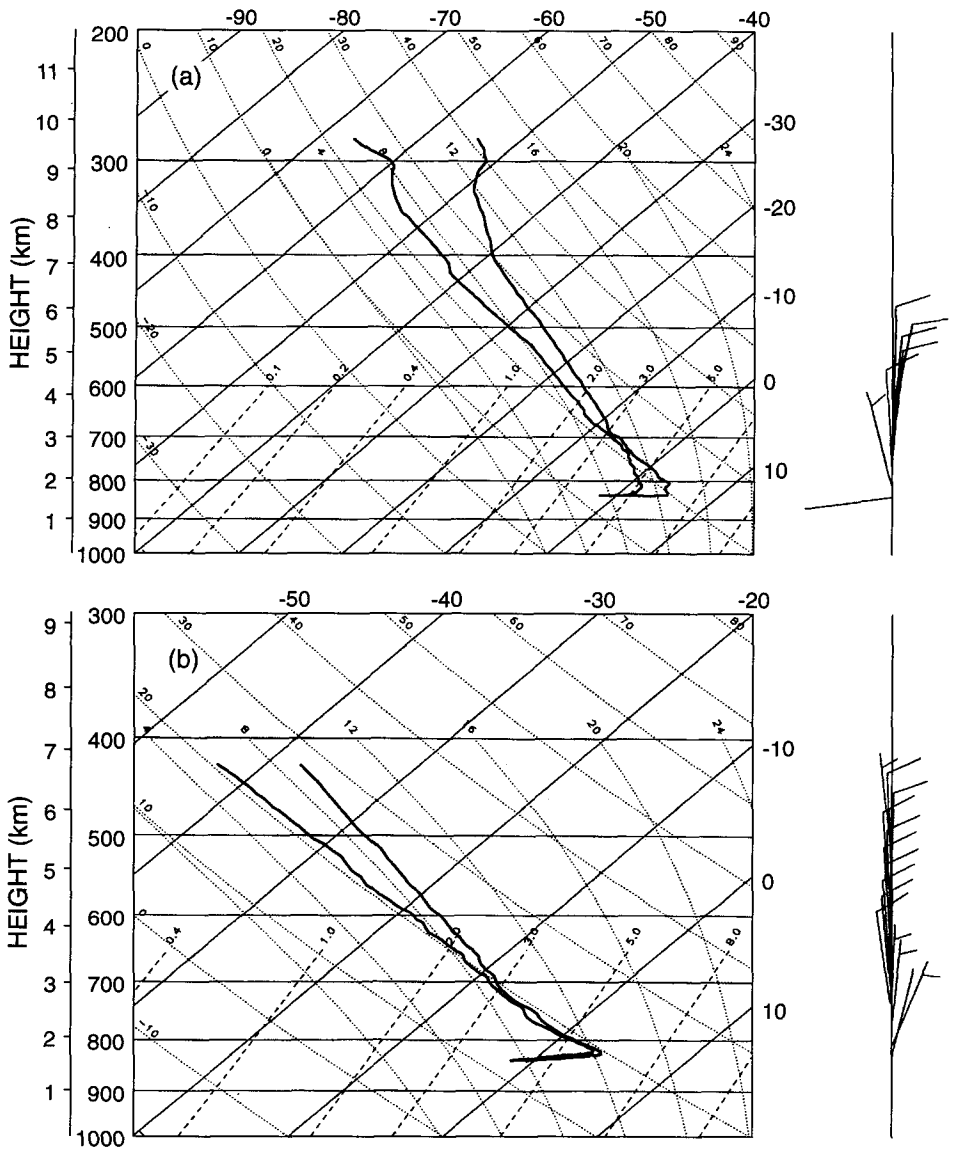

FIG. 8. (a) Skew-*T* plot for CLASS sounding at Berthoud (BTD) 0414 UTC 16 January. On the vertical wind profile on right, one barb equals 10 m s^{-1}. Temperature and dewpoint profiles are the solid lines. Also lines of constant temperature, potential temperature, equivalent potential temperature, and mixing ratio are lightly drawn. (b) As in (a) but for 0610 UTC.

from 3 to 4.5 km; concentrations above 12 L^{-1} were found at heights up to 5.0 km. Ice crystals up to 6 mm in diameter were located in the lower portions of the cloud (Fig. 11e). The position of the unstable region, high crystal concentrations, largest crystal sizes, and liquid water match the dual-Doppler data closely, when the radar data are appropriately shifted northward. Ascending flow within the convectively unstable region formed high crystal concentrations that grew rapidly as they fell within the high-reflectivity area, and small amounts of liquid formed at the leading edge of the band where ice crystals were not able to deplete the liquid by riming. The northern edge of B2 was well defined during this period, with drier, precipitation-free air located just north of the band within a region of band-relative rear inflow. This feature agreed with the available surface reports of a temporary termination of snowfall after passage of B2.

The maximum surface convergence shown in Fig. 6c would produce an updraft of only about 0.05 m s^{-1}, based on continuity using a representative depth of 500 m. Using the slopes of the θ_e surfaces in Fig. 11b, upglide along these surfaces with an inflow of 5 m s^{-1} would produce a vertical velocity of 0.3 m s^{-1}, or a

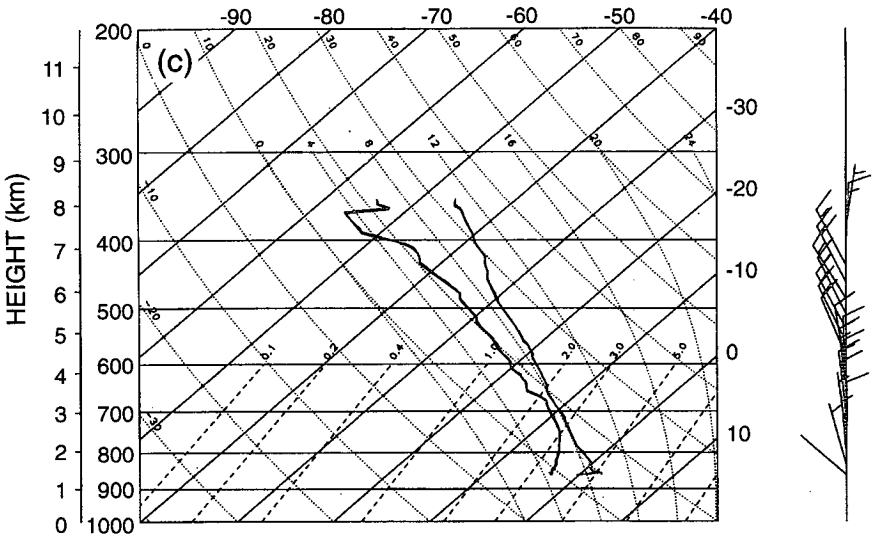

FIG. 8. (*Continued*) (c) As in (a) but for the 0614 UTC launch at Wiggins (WIG).

factor of 2 less than the dual-derived velocities in Fig. 10. Thus it is certainly possible that convection was significant and contributed to the updraft, given the lack of significant larger-scale lifting in this case and the presence of low-level convergence. Soundings measured in the vicinity of the band supported this scenario, as discussed previously.

The MHR reflectivity scan at 0829 (Fig. 9c) showed the axis of the east–west-oriented band B2 to be located 30 km south of MHR at that time. The reflectivity north of this band had decreased rapidly, and most of the northern half of the WISP domain was free of echoes above 5 dBZ. DEN reported light snowfall (1-mile visibility) at 0752, moderate snowfall ($^1/_2$ mile) at 0758, heavy snowfall ($^1/_{16}$ mile) at 0804 with northerly gusts to 9 m s^{-1}, and light snow showers at 0818 through 0824. The band moved south of DEN by 0900, and appeared to dissipate both in size and magnitude. Light snowfall at DEN ended by 0831, and only fog was reported thereafter until 1300. The trend toward precipitation-free conditions in the WISP domain began in the northern portion with the exit of B2 and continued until nearly 1100, when another west-northwest–east-southeast band (B3) began to form rapidly near GLY. Here B3 evolved similarly to B2 but exhibited lower maximum reflectivity values. It is likely that the dissipation in radar echoes after 1400 over northeastern Colorado was due to the low-level dry air advection from the north noted previously.

c. Additional MHR radar data analyses

Examination of MHR radar reflectivity movie loops of plan position indicator (PPI and RHI) scans from 0000 to 1600 UTC 16 January (at 0.5° and 1.2° elevation angles) indicated a preferred, roughly north–south zone of reflectivity intensification over the western South Platte River valley, extending from the foothills west of DEN, BOU, and FCL on the west side, eastward about 50–70 km, including PTL. This time period spanned the lifetime of all three bands B1–B3. It is unlikely that the either the 0.5° or 1.2° scans were overshooting significant precipitation features within 150 km of the radar, given the convective nature of the precipitating clouds. Generally, echoes entering this zone from the north intensified by approximately 10–25 dBZ within 0.5–1.5 h, organized into bands and persisted until they exited the zone. Rapid weakening was observed once the bands reached the area just south of DEN despite the presence of low-level upslope flow. For example, maximum reflectivities within band B2 increased from about 10 dBZ near CYS to well over 30 dBZ near DEN before they rapidly weakened south of DEN. Reflectivity in and near the foothills west of FCL, BOU, and DEN was much more persistent between bands than that over the plains.

These observations are readily evident on the plot of the average reflectivity from MHR at 1.8 km AGL CAPPI for the 0437–0858 time period in Fig. 12 (corresponding with the period of the time average of winds shown in Fig. 7). Transient, propagating bands were essentially removed by time averaging, while stationary effects were retained, thus revealing enhanced reflectivity caused by the LA. As shown, over and slightly south of the aforementioned zone of band intensification, 20–30-dBZ averages were present over and adjacent to the foothills from just southwest of FCL to southwest of DEN (the foothills themselves were removed from the analysis). Thus it is apparent that reflectivity between bands was important in this region. Eastward extension of the high reflectivity values was evident over and just north of DEN. Snowfall rates of light to occasionally moderate

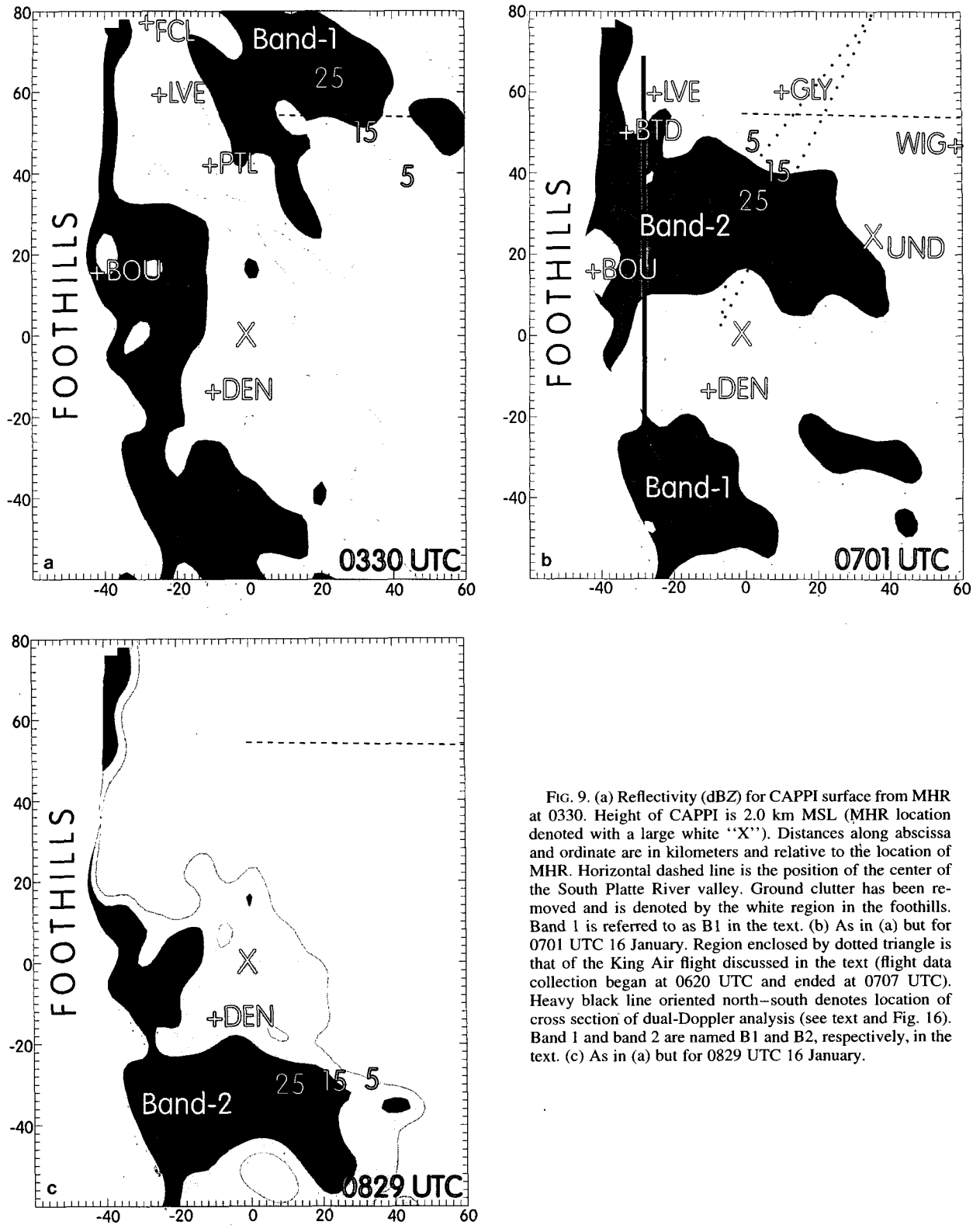

FIG. 9. (a) Reflectivity (dBZ) for CAPPI surface from MHR at 0330. Height of CAPPI is 2.0 km MSL (MHR location denoted with a large white "X"). Distances along abscissa and ordinate are in kilometers and relative to the location of MHR. Horizontal dashed line is the position of the center of the South Platte River valley. Ground clutter has been removed and is denoted by the white region in the foothills. Band 1 is referred to as B1 in the text. (b) As in (a) but for 0701 UTC 16 January. Region enclosed by dotted triangle is that of the King Air flight discussed in the text (flight data collection began at 0620 UTC and ended at 0707 UTC). Heavy black line oriented north–south denotes location of cross section of dual-Doppler analysis (see text and Fig. 16). Band 1 and band 2 are named B1 and B2, respectively, in the text. (c) As in (a) but for 0829 UTC 16 January.

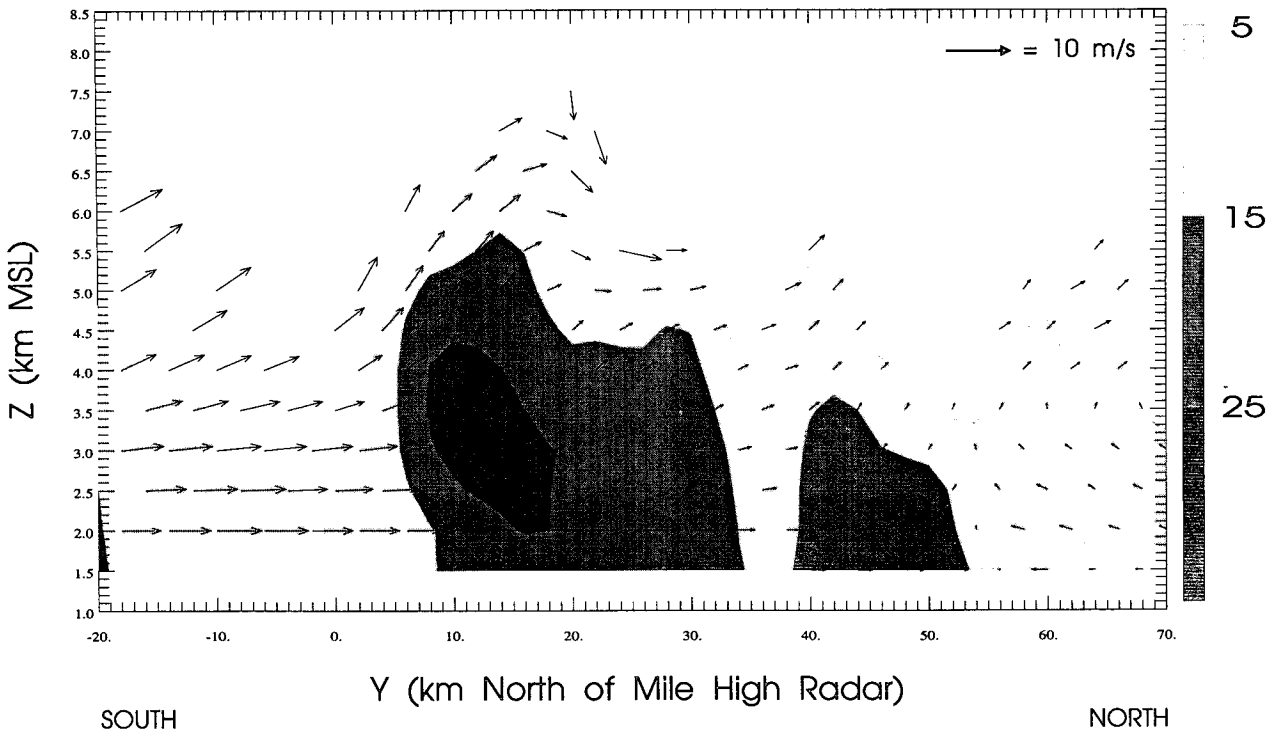

FIG. 10. North–south vertical cross section of dual-Doppler-derived velocities and reflectivity at 0705 UTC 16 January, 28 km west of MHR, through snowband B2. Horizontal velocities are band relative. Vertical velocities were calculated using upward integration of the convergence field.

(and heavy in portions of B2) intensity were associated with this area of enhanced reflectivity. Also, averaged reflectivity values decreased southeast of Denver, despite the fact that northerly winds were upslope in nature on the north slope of the Palmer Divide.

Analysis of snowfall accumulation from a volunteer observer network (Fig. 13) (Bernstein et al. 1992), showed very good correlation in both magnitude and spatial distribution with the time-averaged reflectivity field (Fig. 12). Heaviest snowfall (6–9 cm) occurred over and west of DEN and BOU, just south of the LA region; significantly less (0–4 cm) snow fell to the north and east of this zone. No significant snow-producing features were observed outside of the preferred region of intensification within the WISP domain. Low-level winds during this event were generally less than 10 m s^{-1} in the region of heavier accumulation and higher reflectivities were confined to the lowest 2 km or so. Thus the locations of persistently intense reflectivities exhibited little difference from those of significant snowfall. Generally, incoming weak echoes intensified over the western South Platte River valley and propagated southward before dissipating over the north slopes of the Palmer Divide. Accordingly, heaviest snow amounts were located from near Denver to just north of Boulder.

Examination of movie loops of RHIs and PPIs corroborated the scenario that the convergent region and convective instability over the northwest portion of the WISP domain led to rapid intensification and deepening of weak echoes propagating into the area from the north. Close examination of Figs. 12 and 7b revealed a discrepancy in the location of the averaged maximum reflectivity and the maximum low-level convergence. The latter was located about 50 km to the north of the former. The LA-induced convergence appears to be triggering convective instability over the FCL–LVE area, but some amount of time is required for the hydrometeors produced in the updraft to be realized as precipitation. The time required for crystals to grow to large (i.e., precipitation) sizes and fall to the ground likely accounted for the difference in location between maximum convergence and low-level reflectivity. Snowflakes producing 25–35-dBZ reflectivities would require timescales on the order of at least 10–20 min to grow to large sizes. A reasonable estimate of time required for fallout from heights of 1–2 km, the typical location of initial reflectivity intensification according to the RHIs in this case, is 20–30 min. Given the ambient 2-km AGL wind speed of about 10 m s^{-1}, total horizontal southward displacement of initial convectively induced hydrometeors prior to landfall could easily be 30 km or more.

5. Mesoscale model experiments

To further examine the detailed characteristics of low-level northerly flow along the Colorado Front

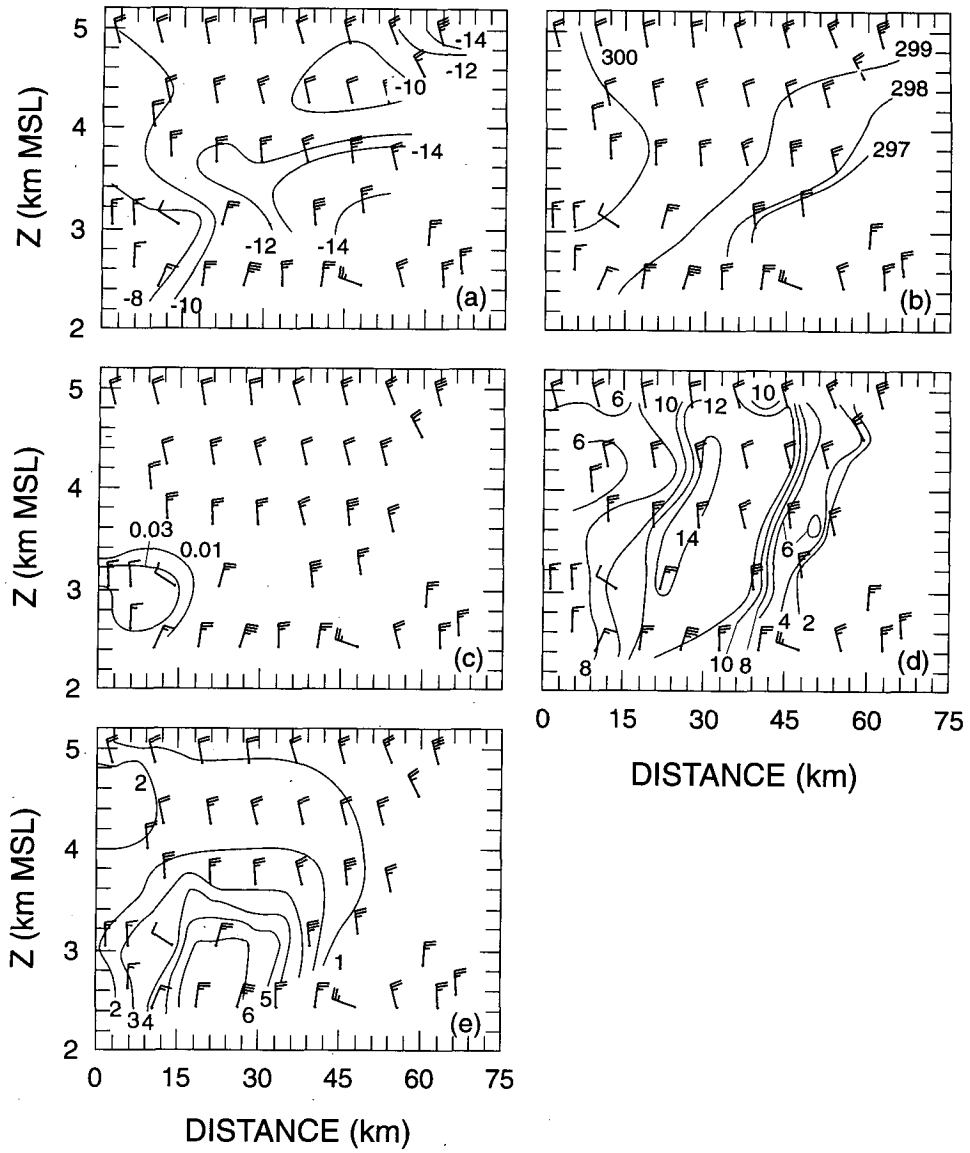

FIG. 11. King Air measurements for the 0620–0707 UTC 16 January flight. Vertical cross sections are oriented at 030°. Flight location is shown in Fig. 9b. Origin of plot corresponds to the southernmost point of the triangular region denoted on Fig. 9b. Data are distance-adjusted to account for movement of the snowband during the flight. Winds measured are shown on the plot; one barb equals 5 m s^{-1}: (a) v wind component (m s^{-1}), (b) θ_e (K), (c) liquid water content (g kg^{-1}), (d) ice crystal concentration (L^{-1}), (e) maximum ice crystal diameter (mm).

Range, a series of numerical simulations was conducted using the Colorado State University Regional Atmospheric Modeling System (CSU RAMS) (Pielke et al. 1992). The intent of the simulations was to isolate and better assess the effects of the terrain on local horizontal and vertical motion fields during northerly wind episodes. The results allow generalizations to be made for terrain-induced vertical motion during northerly winds and further insight into snowfall mechanisms through comparison with the observational case study results. In addition the numerical results could be applied to other regions of complex terrain since a generic initial state was utilized.

The RAMS model simulations performed in this study utilized a three-dimensional, nonhydrostatic, nested version of RAMS (see Table 1 for the details of model characteristics for these simulations) with detailed topography. To better simulate the effects of the Cheyenne Ridge and the other topographic features in the WISP domain, a third nested grid was centered on

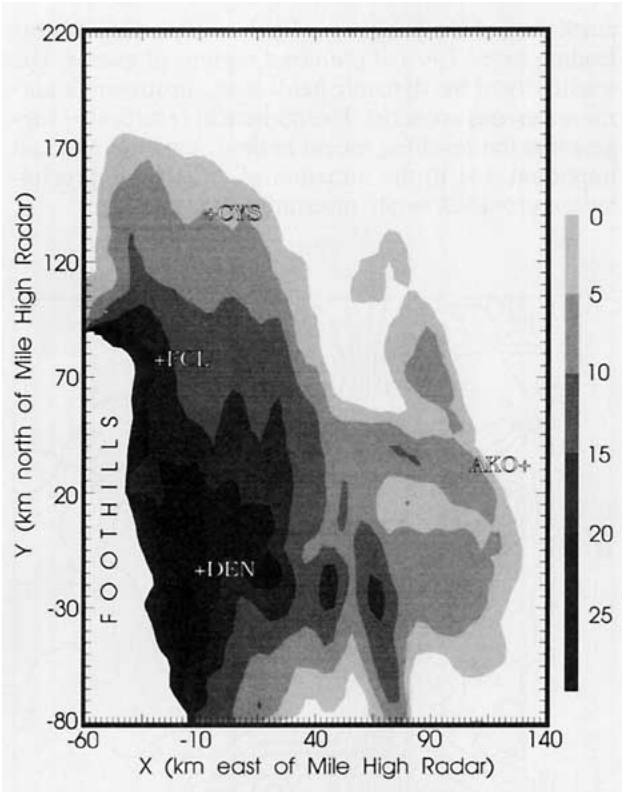

FIG. 12. Time average of MHR reflectivity between 0437 and 0858 UTC 16 January for the 3.3-km MSL CAPPI. Ground clutter caused by the foothills and other topographic features has been removed.

the area (see Fig. 14a); it contained a horizontal grid spacing of 2.5 km.

To examine terrain effects in detail, while matching observed initial conditions as closely as possible, the model was initialized with a single sounding (shown in Fig. 14b) so that the model fields were initially horizontally homogeneous. This sounding was constructed based on the authors' best estimate of a representative lapse rate and wind profile (given the available WISP sounding data shown in Fig. 8) likely present upstream of the Cheyenne Ridge during the developmental portion of the 16 January 1991 Longmont anticyclone event. The initial wind profile contained north-northwesterly flow at 10 m s^{-1} through the troposphere.

Figures 15a and 15b present the winds at the lowest model grid level (48 m above the ground surface) at 6 and 10 h of the simulation. Clearly, the Longmont anticyclone and its associated deceleration are well developed at this time. An area of significant anticyclonic turning has formed north-northeast of Boulder, in approximate agreement with the documented regions of the 16 January 1991 event (see Fig. 7). Convergence of westerly flow in the foothills with weak northeasterly flow over the plains is also evident. The vertical motion field at a height of 420 m, shown in Fig. 15c at 6 h of simulation, indicates that a strong updraft has formed over the area of turning and convergence, with a maximum speed of 0.9 m s^{-1} located approximately 30 km north of Boulder (BOU). The plains to the east of the mountains are characterized by very weak vertical motions, while significant descent covers much of the foothills. The pattern of strong upward motion, anticyclonic turning, and low-level convergence was persistent in the simulation; a quasi-steady state in the dynamic fields was present between approximately 2 and 12 h of simulation.

A series of sensitivity simulations, modifying the lapse rate of the initial sounding, was conducted in order to further investigate topographic effects on northerly winds in the Front Range. Figure 16 summarizes the results of these tests. The initial upstream Froude number (Fr = $UN^{-1}h^{-1}$, where U is the wind velocity, N is the Brunt–Väisälä frequency, and h is the effective mountain height calculated for flow impinging on the Cheyenne Ridge) is plotted against the maximum predicted updraft speed within the third nested grid. Generally Fr values in the 0.5–2.0 range are associated with the blocked flow regime, in which winds tend to be diverted around obstacles. In the simulation just described, Fr = 0.9. In the successive three experiments, Fr values were 1.4, 2.0, and 7.0, respectively. The Fr

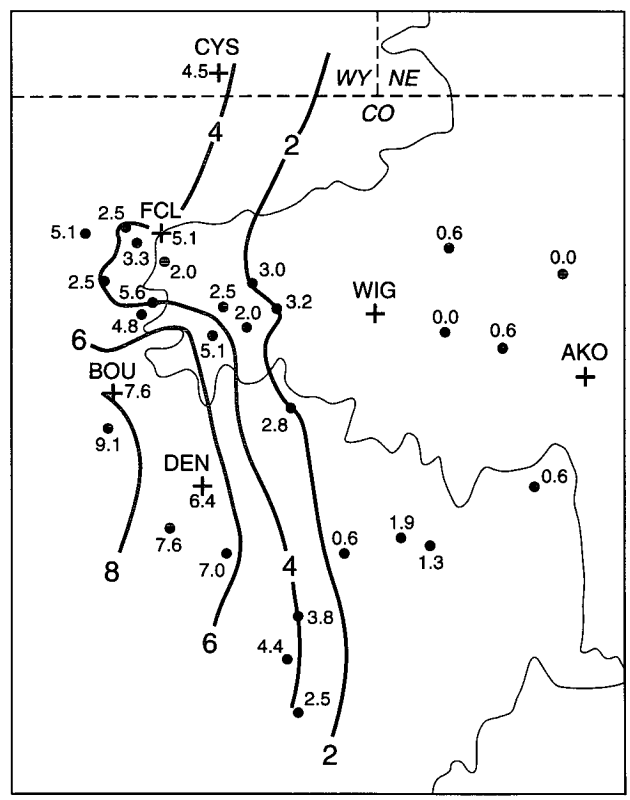

FIG. 13. Snowfall reports (cm) for the 16 January 1991 event from the WISP observer network, standard National Weather Service (NWS) reports, and NWS cooperative observer measurements.

TABLE 1. RAMS simulation description for 16 January 1991 study.

Model category	Option used
Equations	Primitive; nonhydrostatic
Initialization	Single sounding (see Fig. 14b) uniform winds at 340°, 10 m s^{-1}
Coordinate system	Lat–long and sigma
Top boundary condition	Rayleigh friction
Height of model top	16 km
Lateral boundary conditions	Radiative
Boundary layer parameterization	Vertical eddy flux parameterization (see Louis 1979) and prognostic soil model (see Tremback and Kessler 1985)
Thermodynamics	No condensation
Radiative effects	Longwave and shortwave parameterizations
Horizontal grid spacing/size	Grid 1: 30 km/60 points Grid 2: 7.5 km/50 points Grid 3: 2.5 km/50 points
Vertical grid spacing/size	100 m at ground, stretched to 500 m above 10 km/37 levels
Topography	Silhouette-averaged using 30-s data
Time step	Grid 1: 60 s Grid 2: 15 s Grid 3: 5 s

was modified by changing only the initial lapse rate (and thus changing N) in the lowest 1500 m of the atmosphere; initial winds were identical in all experiments. A well-developed LA occurred in the second simulation. A weaker LA developed in the third experiment, but terrain effects were negligible in the last case. As shown in Fig. 16, the maximum updraft strongly decreases as Fr increases. There is also tendency for reduced updraft sensitivity for higher Fr's. In the three lower-Fr cases the maximum updraft was positioned directly in the preferred LA region discussed previously, whereas in the Fr = 7.0 case there was no significant area of updraft over the entire inner grid. In all of the simulations a quasi-steady state was reached after about 2 h. The tendency for air to resist ascent up and over the Cheyenne Ridge for low Fr apparently leads to flow around the obstacle at lower elevations, creating the leeside negative vorticity, convergence, and updraft (Smith 1979; Snook 1993; and Crook et al. 1990). In southeastern Wyoming during wintertime, a typical value of Fr for northerly flow is less than 1.0, well within the blocked flow regime. Synoptic-scale northerly low-level flow is also a common occurrence in this region.

These results strongly suggest that the development of the LA is closely tied to the effects of topography. The immediate, persistent, and pronounced appearance of low-level convergence, anticyclonic turning, and significant updraft in idealized model simulations initialized with a single sounding, and the agreement in the location of these features with the convectively initiated snowfall documented for 16 January 1991, suggest that the upstream higher terrain to the north and northwest of the region are likely the primary factors leading to the LA and preferred regions of ascent. The sensitivity of the dynamic fields to the upstream Fr corroborates this scenario. The numerical results also suggest that the resulting ascent in the LA region plays an important role in the initiation of clouds and precipitation, provided ample moisture is present.

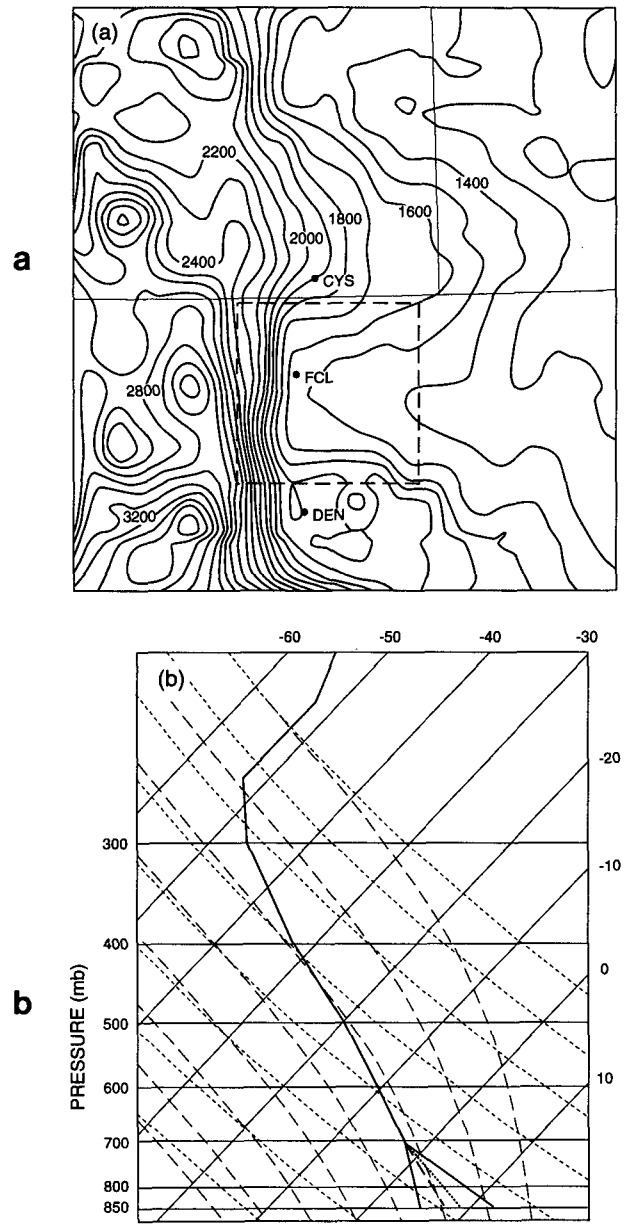

FIG. 14. (a) Model elevation (m) for grid 3. The area inside the dashed box indicates the plotted region for Fig. 15. (b) Model initial sounding. The four profiles indicate the four different experiments. The first experiment described in the text (Fr = 0.9) is the most stable profile of the four shown. Also drawn lightly are lines of constant temperature (°C), potential temperature, and equivalent potential temperature.

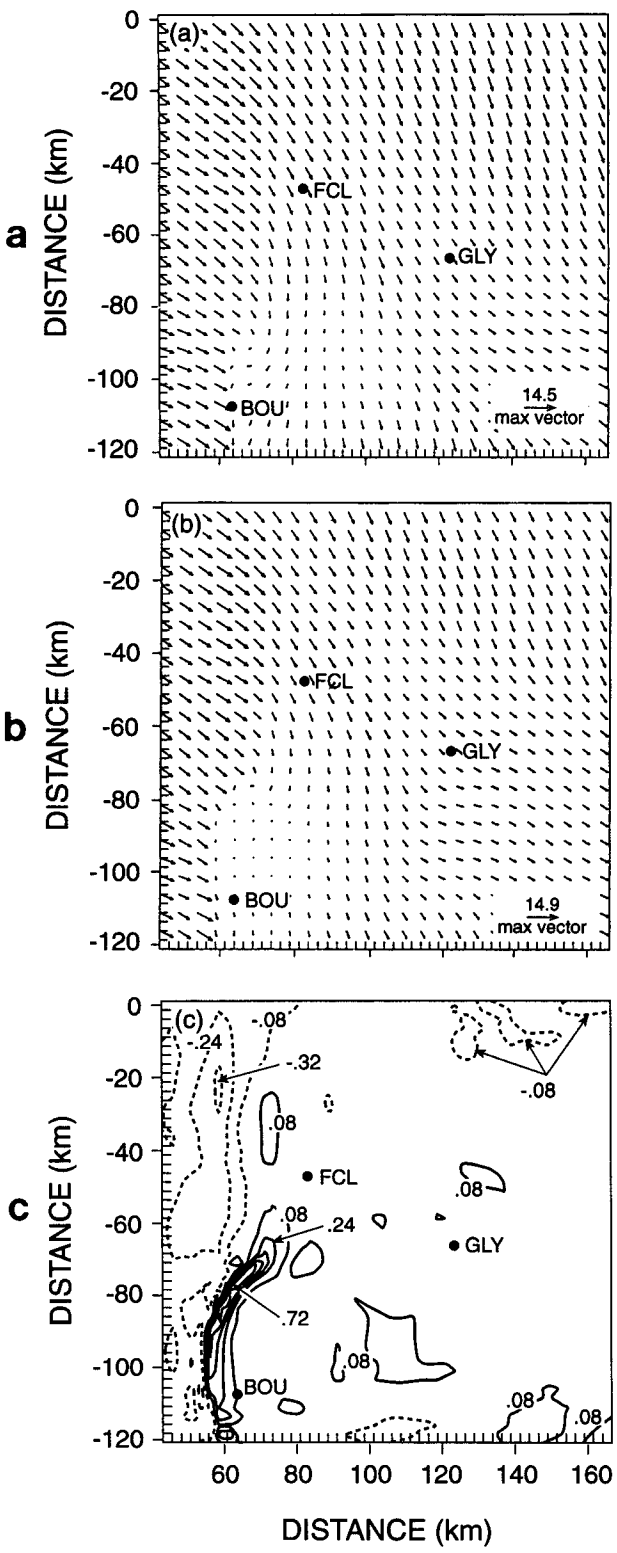

FIG. 15. (a) Model-predicted winds at 6 h of simulation at the model lowest level (48 m). The maximum speed of the inset is in meters per second. (b) As in (a) but at 10 h of simulation. (c) Model-predicted vertical motion (m s^{-1}) at 6 h of simulation at a model height of 420 m.

6. Discussion of possible formative mechanisms

The surface wind features discussed in this paper are related to the complex topography found in this region (see Fig. 1), and lead to significant snow production over and near the foothills northwest of Denver. It is probable that the anticyclonic turning in the low levels of the atmosphere is caused by negative vorticity generation on the left lee side of a three-dimensional obstacle (the Cheyenne Ridge in this case) during low–Froude number flow (Crook et al. 1990; Smolarkiewicz and Rotunno 1989; Snook 1993). However, the lack of observational data (i.e., wind and lapse rate profiles) in this case over and upstream of the Cheyenne Ridge prevented a comprehensive assessment of this scenario. Idealized modeling experiments described in the previous section reproduced the LA feature and the associated preferred region of ascent. There is also an indication in the wind analysis in this case (Fig. 7a) and in the model simulations (Fig. 15a) that convergence between the northeasterly flow over the western South Platte River valley and westerly winds in the foothills west of BOU may be important to the enhancement of snowfall.

a. Delay of low-level cold advection

The high-resolution surface and sounding measurements for this LA occurrence on 16 January 1991 enabled the role of small-scale variations in lapse rates to be assessed. The cellular reflectivity patterns observed in this event, as well as the presence of significant echoes up to the 5.5-km level and aircraft measurements of convective instability, warranted a close look at the

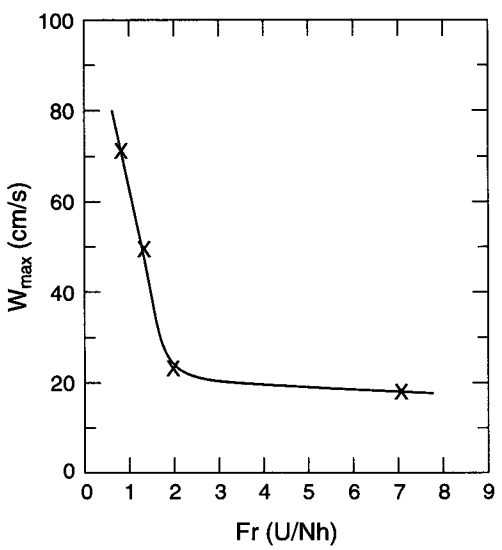

FIG. 16. Results of model sensitivity experiments. Froude number Fr (see text) is plotted on the ordinate. The maximum upward motion plotted on the abscissa refers to that of the entire grid 3 in the simulation.

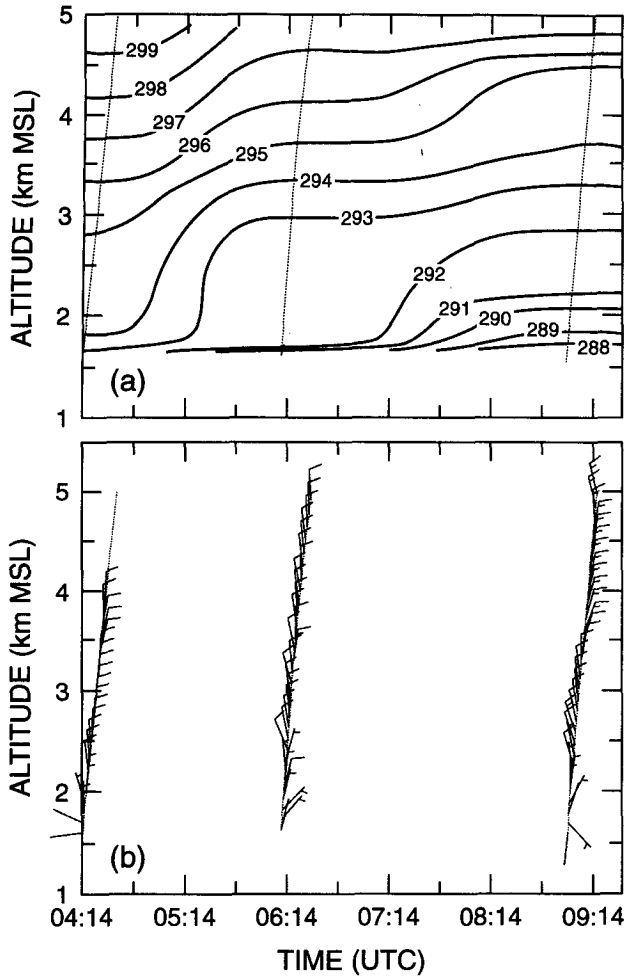

FIG. 17. Time–height cross section of three BTD CLASS soundings: (a) potential temperature (K); (b) winds. One wind barb corresponds to 5 m s^{-1}.

role of convection in the development of precipitation. Between 0300 and 0600 UTC (the developmental LA stage) CLASS measurements at HUD and AKO indicated significant cooling from the surface to 700-mb, in response to the postfrontal cold advection discussed in section 3b. Cooling (2°–3°C) was strongest at both locations between 0300 and 0600. However, the low-level cold advection was nearly zero at BTD before 0700 (see the time–height cross section in Fig. 17). As shown by analyzed mesonetwork wind observations (Fig. 7a), this region exhibited much lower wind speeds in the lower troposphere, as is typical during an LA. Warmer conditions also characterized this area (Fig. 6b). *Above 700-mb, however, all of the locations exhibited little difference in the magnitude or timing of cold advection.*

As discussed previously, the BTD sounding at 0610 UTC revealed a nearly dry-adiabatic temperature profile from above the surface-based inversion to nearly 700 mb. This layer was also nearly saturated, although as discussed in the appendix the low-level relative humidity values may have been somewhat overestimated. However, the three sounding sites to the east, HUD, WIG, and AKO, all measured significantly different profiles at 0600 UTC. The HUD low-level lapse rate was absolutely stable between the surface and 750 mb, and generally moist adiabatic above that level. At WIG (Fig. 8c), the lapse rate between the surface and 600 mb was approximately moist adiabatic, aside from a slightly unstable 30–40-mb-deep layer near the ground. Finally, at AKO the lapse rate was approximately moist adiabatic in the lowest 80 mb or so, then slightly unstable from 750 to 600 mb. Only BTD had any significant layer of temperature above 0°C.

Figure 18a shows a vertical cross section of θ_e oriented east–west at 0600 for the BTD, HUD, and AKO soundings. The convective instability at BTD between approximately 1.8 km and nearly 3 km is immediately evident and exists due to the warmer and more moist conditions at BTD. Again, the θ_e values in the lowest

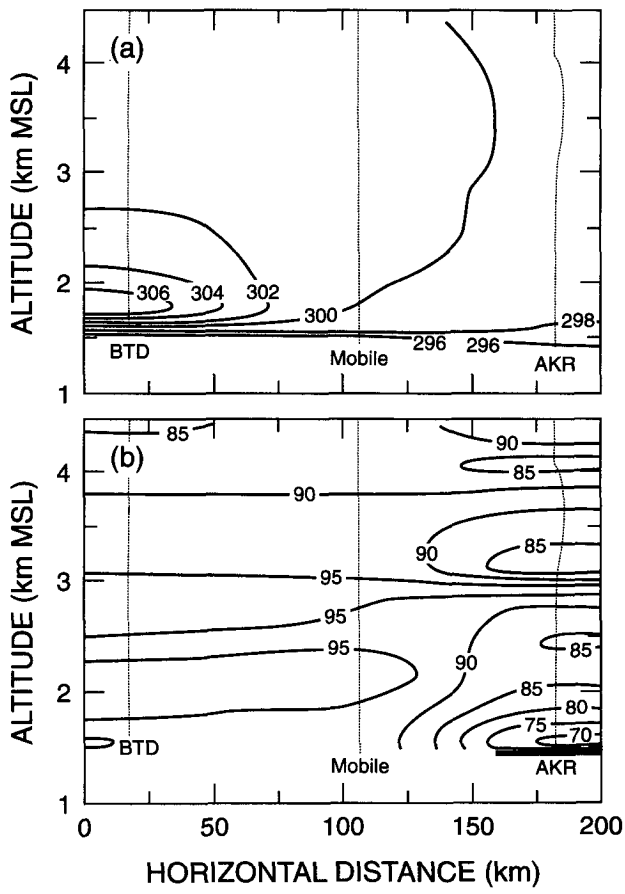

FIG. 18. (a) Vertical cross section of equivalent potential temperature (K) for the BTD, HUD (mobile), and AKO CLASS soundings at approximately 0600 UTC 16 January. (b) Relative humidity (%) cross section for the soundings shown in (a) at 0600 UTC.

1 km at BTD may have been overestimated due to icing of the humidity sensor (see appendix). However, even a fairly large reduction (e.g., 30%) in humidity in this layer would not have eliminated the convectively unstable conditions. On the other hand, the HUD (mobile) and AKO profiles are convectively stable. The aircraft profile of θ_e discussed previously specified a layer of convective instability within band B2 when it was located just south of BTD. The flight was conducted about 40 km east of BTD. The vertical cross section of relative humidity at this time (see Fig. 18b) shows the more moist conditions at BTD. This tendency for relatively warm, moist low-level conditions to be observed only over the western end of the South Platte Valley lasted past 0800. Temperatures in the 800–700-mb layer still averaged about 2°C warmer at BTD than those at WIG and AKO at 0900.

The apparent cause of this temperature gradient in the surface-to-700-mb layer is related to differences in the time of onset of low-level postfrontal cold advection between the western South Platte River valley and the eastern Colorado plains. As discussed in section 3, the western South Platte River Valley was characterized throughout most of this event by light northeasterly winds. Winds from the surface up to about 2 km AGL were significantly weaker over the foothills northwest of Denver and over the western South Platte Valley due to the presence of the LA. It is apparent from the soundings at BTD and those taken to the east that while low-level (surface to approximately 700 mb) cold advection stabilized HUD, WIG, and AKO between 0300 and 0600, stabilization did not begin at BTD until 0700. The average wind speed in the lowest 1.0-km layer at AKO more than doubled that at BTD, and was about 50% greater than the HUD wind speeds. The average wind direction in this layer was approximately 330°, compared to 0° at BTD. This delay in significant cooling, caused by an east–west gradient in low-level temperature advection, in combination with ample low-level moisture and convergence, led to convection over the west end of the South Platte River valley. Since conditions aloft were nearly identical in this region, destabilization occurred in the BTD area.

b. Surface pressure analyses

Surface pressure measurements revealed some interesting mesoscale variations. On the larger scale, a gradient in MSL pressure directed northwest to southeast extended from central Wyoming to southeastern Colorado and western Kansas at 0700 (see Fig. 5a). The analyzed mesonetwork surface pressures, shown in Fig. 5b for 0500 and discussed previously, showed that the CYS–GLY–FCL region, where the LA signature was developing, exhibited little to no pressure gradient, while east and south of Greeley the northwest–southeast gradient was present and of at least the same magnitude as the large-scale gradient. The region of decreased pressure gradient may have been the result of leeside low pressure enhancement (e.g., Ferber and Mass 1990). Similar pressure gradient patterns have been observed in other WISP studies of the LA (C. Davis 1995, personal communication). The pattern began to develop between 0200 and 0300 UTC 16 January 1991, and persisted for some time until after 0700. The presence of the pattern in the pressure gradient closely corresponded temporally to the developmental phase of the LA feature. As discussed above, reduction of flow velocity by the LA reduced the cold advection in the western South Platte River valley, which hydrostatically inhibited the larger-scale pressure rises, contributing to the adjusted pressure gradient shown in Fig. 5b. The case study results and the numerical simulations indicate that the response of the low-level flow to higher terrain northwest of this region in a low-Fr regime leads to a strong reduction in wind speeds on the lee side.

7. Conclusions

The Longmont anticyclone (LA) is a local feature downstream of a modest, sloping east–west ridge, and is typically characterized by low-level convergence and anticyclonic turning within ambient postfrontal northerly flow, in contrast to the Denver cyclone, which forms within ambient southerly or southeasterly winds. Winter Icing and Storms Project (WISP) measurements, both at the surface and aloft, were analyzed in detail for the event of 16 January 1991 in northeastern Colorado. In this case the LA was present for more than 10 hours and featured low-level convergence, snowfall, and snowbands. Snowfall rates were occasionally moderate to heavy. Unlike typical Denver cyclone cases, the low-level winds did not exhibit organized return (i.e., southerly in this case) flow. Snowband propagation was approximately 10–12 m s^{-1} to the south, and the strongest band resembled a long-lived convective line. To the east of the WISP domain, little or no snowfall was reported during this event, while 5–9 cm accumulated in the western and southwestern portions of the domain. Synoptic-scale forcing was considered weak. Surface measurements in this storm indicated highly ageostrophic low-level wind components, though not of the same magnitude as in the Johnson et al. (1984) case study. Based on detailed examinations of low-level radar reflectivity scans during the snowy period of 0000–1200 UTC 16 January, a preferred zone of reflectivity intensification was located over the western South Platte River valley. This region was located just downstream of the area of highest convective instability and low-level convergence (as specified from time-averaged wind fields) and was verified using time averaging of reflectivity scans.

A series of nested mesoscale model simulations using the CSU RAMS demonstrated the development of a significant updraft within a region characterized by

anticyclonic turning and reduced wind speeds in the same area as the observed LA. The simulations were initialized with a single sounding derived from the observed WISP soundings; similar lapse rate and wind characteristics to this sounding are frequently observed in this region. The location of the convergent region exhibited agreement with that of the case study. Significant ascent over the northeastern Colorado region was confined to the western Platte River valley. Numerical sensitivity experiments altering the initial stability in the model fields revealed a strong dependence of updraft strength on the stability. More stable conditions (lower Froude number) produced a stronger updraft. These findings strongly suggest that the occurrence of the LA is a terrain-forced event and may indeed be forecastable, given an estimate of upstream stability and winds. The high frequency of LA events during WISP corroborates the scenario of terrain-forcing of the LA during northerly flow as described by the simulations.

Mesonet data and numerical simulations indicated that direct mechanisms leading to mesoscale upward motion in association with the LA are the following:

1) Convergence of northerly flow over the Cheyenne Ridge with weak northeasterly or calm winds in the western portion of the South Platte River valley.

2) Convergence of westerly flow in the foothills northwest of Denver with weak northeasterly or calm winds over the western South Platte River valley.

An indirect mechanism for mesoscale upward motion in the case study was an east–west gradient in low-level thermal advection between the area of lighter winds over the west end of the South Platte Valley and the area of stronger winds over the plains to the east. Convectively unstable conditions were observed only over the western South Platte Valley. This area appeared to retain warm, moist low-level conditions and weak winds during a period of large-scale advection of cooler and drier air. The weak winds are inherently a part of the LA wind pattern and cause a delay in cold advection. The LA-induced precipitation intensification led to maximum enhanced snowfall approximately 50 km south of the maximum surface convergence in an environment characterized by northerly midlevel winds.

The unimpeded low-level north-northwesterly flow over the plains to the east of the LA region strongly inhibited cloud and precipitation formation, as drier and more stable upstream conditions quickly replaced the air mass in the vicinity of the cold front. It is plausible that the anticyclonic turning associated with the LA can be explained by negative vorticity generation on the downstream left side of a three-dimensional obstacle, the Cheyenne Ridge. The presence of a reduced surface pressure gradient over the western South Platte River valley corresponded with the warm and decelerated portion of the anticyclonic LA wind pattern. The relative importance of low-level convergence in generating precipitation as opposed to convective instability caused by gradients in thermal advection is unclear at this time, although convection appeared to be critically important in this event. The results of this study suggest that LA-induced ascent could be important during heavier snowfall events. However, the exact nature of the role of the LA during cyclonic events will require further analysis of WISP datasets, and additional numerical model simulations.

Acknowledgments. This work was funded by the FAA Grant DTFA01-90-Z-02005. The authors benefited from helpful discussions with Roger Pielke, Jim Toth, John Brown, Jerry Schmidt, John Snook, Dave Kingsmill, and Ed Szoke. Marcia Politovich is thanked for providing a helpful review of the manuscript. Peter Neilley, Ian Baker, and Ben Waite assisted with portions of the data analysis. Jeff Cole, Dan Megenhardt, Valerie Scheele, Carol Makowski, Justin Kitsutaka, and others at NCAR graphics provided assistance with portions of the drafting and text preparation.

APPENDIX

Possible Errors in BTD Sounding Data

The observations in Fig. 8b of nearly saturated (with respect to water) conditions in regions characterized by a dry-adiabatic lapse rate warranted a closer look at the BTD instrumentation. The CLASS radiosondes, manufactured by Vaisala, measure relative humidity using a dielectric material, and are subject to extensive calibration during preparation (C. Wade, NCAR 1994, personal communication). The humidity sensor is protected against raindrops by using a cap as well as special treatment with a water-repellent substance. Due to icing, however, the humidity sensor may record anomalously high relative humidity values. Several relevant weather observations in the vicinity of snowband B2, a portion of which was located over BTD during the 0610 sonde flight, were logged. First, at 0610 cloudy and snowy conditions were observed visually. Second, GOES infrared imagery measured cloud-top temperature of approximately −20°C above BTD, which according to the sounding in Fig. 8b corresponded to about 570 mb. These findings indicated that the lower portion of the troposphere at this time was likely characterized by relative humidity values above 75%, assuming of course that the intermediate region between about 700 and 600 mb was cloudy (note: at AKO, where snow was not falling, this layer exhibited relative humidity values of 82% or greater at this time). The third relevant observation in this region was that many of the crystals examined at the surface below band B2 were heavily rimed, supporting the possibility that icing of the humidity sensor did occur and led to the high relative humidities shown in Fig. 8b.

Despite the possibility that the CLASS data overestimated the actual relative humidities at BTD, values

above 75% were likely present in the 800–600-mb layer. Given this likelihood and the measurements of an unstable low-level temperature profile at BTD, convective instability in the 820–700-mb layer was present and was likely of significant magnitude even if the humidity values were overestimated. The combination of the measured lapse rate and a hypothetical minimum humidity of 60%–70% would still have created convectively unstable conditions. (Note: as opposed to possible errors in relative humidity measurements, the temperature profiles in these sondes exhibit a very high degree of accuracy.)

REFERENCES

Akaeda, K., J. Reisner, and D. Parsons, 1995: The role of mesoscale and topographically induced circulations in initiating a flash flood observed during the TAMEX Project. *Mon. Wea. Rev.*, **123,** 1720–1739.

Bernstein, B. C., I. Baker, D. Wesley, J. Smart, L. Wharton, and J. Wirshborn, 1992: The utility of a high resolution volunteer snow observer network. *Proc. 11th Int. Conf. on Clouds and Precipitation,* Vol. 2, Montreal, PQ, Canada, ICCP/IAMAP, 991–994.

Crook, N. A., T. L. Clark, and M. W. Moncrieff, 1990: The Denver cyclone: Part I. Generation in low Froude number flow. *J. Atmos. Sci.,* **47,** 2725–2742.

Ferber, G. K., and C. F. Mass, 1990: Surface pressure perturbations produced by an isolated mesoscale topographical barrier. Part II: Influences on regional circulations. *Mon. Wea. Rev.*, **118,** 2597–2606.

Johnson, R. H., G. S. Young, J. J. Toth, and R. M. Zehr, 1984: Mesoscale weather effects of variable snow cover over northeast Colorado. *Mon. Wea. Rev.*, **112,** 1141–1152.

Louis, J. F., 1979: A parametric model of vertical eddy fluxes in the atmosphere. *Bound.-Layer Meteor.*, **17,** 187–202.

Marwitz, J. D., and P. J. Dawson, 1984: Low-level airflow in southern Wyoming during wintertime. *Mon. Wea. Rev.*, **112,** 1246–1262.

Nickerson, E. C., and M. A. Dias, 1981: On the existence of atmospheric vortices downwind of Hawaii during the HAMEC project. *J. Appl. Meteor.*, **20,** 868–873.

Pielke, R. A., W. R. Cotton, R. L. Walko, C. J. Tremback, M. E. Nicholls, M. D. Moran, D. A. Wesley, T. J. Lee, and J. H. Copeland, 1992: A comprehensive meteorological modeling system—RAMS. *Meteor. Atmos. Phys.*, **49,** 69–91.

Rasmussen, R. M., and Coauthors, 1992: Winter Icing and Storms Project (WISP). *Bull. Amer. Meteor. Soc.*, **73,** 951–974.

Reisner, J. M., and P. K. Smolarkiewicz, 1994: Thermally forced low Froude number flow past three-dimensional obstacles. *J. Atmos. Sci.*, **51,** 117–133.

Smith, R. B., 1979: The influence of mountains on the atmosphere. *Advances in Geophysics,* Vol. 21, Academic Press, 87–230.

Smolarkiewicz, P. K., and R. Rotunno, 1989: Low Froude number flow past three dimensional obstacles. Part I: Baroclinically generated lee vortices. *J. Atmos. Sci.*, **46,** 1154–1164.

——, R. M. Rasmussen, and T. L. Clark, 1988: On the dynamics of Hawaiian cloud bands: Island forcing. *J. Atmos. Sci.*, **45,** 1872–1905.

Snook, J. S., 1993: An investigation of Colorado Front Range winter storms using a nonhydrostatic mesoscale numerical model designed for operational usage. Ph.D. dissertation, Colorado State University, 373 pp.

Szoke, E. J., 1991: Eye of the Denver cyclone. *Mon. Wea. Rev.*, **119,** 1283–1292.

Tremback, C. J., and R. Kessler, 1985: A surface temperature and moisture parameterization for use in mesoscale numerical models. Preprints, *Seventh Conf. on Numerical Weather Prediction,* Montreal, PQ, Canada, Amer. Meteor. Soc., 355–358.

Wilczak, J. M., and T. W. Christian, 1990: A case study of an orographically induced mesoscale vortex (Denver cyclone). *Mon. Wea. Rev.*, **118,** 1082–1102.